4-Aminopyridine-sensitive outward currents in preBötzinger complex neurons influence respiratory rhythm generation in neonatal mice

John A. Hayes, Jeffrey L. Mendenhall, Benjamin R. Brush and Christopher A. Del Negro

Department of Applied Science, McGlothlin-Street Hall, Room 318, The College of William and Mary, Williamsburg, VA 23187-8795, USA

We measured a low-threshold, inactivating K^+ current, i.e. A-current (I_A), in respiratory neurons of the preBötzinger complex (preBötC) in rhythmically active slice preparations from neonatal C57BL/6 mice. The majority of inspiratory neurons (21/34 = 61.8%), but not expiratory neurons (1/8 = 12.5%), expressed I_A. In whole-cell and somatic outside-out patches I_A activated at −60 mV (half-activation voltage measured −16.3 mV) and only fully inactivated above −40 mV (half-inactivation voltage measured −85.6 mV), indicating that I_A can influence membrane trajectory at baseline voltages during respiratory rhythm generation *in vitro*. 4-Aminopyridine (4-AP, 2 mM) attenuated I_A in both whole-cell and somatic outside-out patches. In the context of rhythmic network activity, 4-AP caused irregular respiratory-related motor output on XII nerves and disrupted rhythmogenesis as detected with whole-cell and field recordings in the preBötC. Whole-cell current-clamp recordings showed that 4-AP changed the envelope of depolarization underlying inspiratory bursts (i.e. inspiratory drive potentials) from an incrementing pattern to a decrementing pattern during rhythm generation and abolished current pulse-induced delayed excitation. These data suggest that I_A opposes excitatory synaptic depolarizations at baseline voltages of approximately −60 mV and influences the inspiratory burst pattern. We propose that I_A promotes orderly recruitment of constituent rhythmogenic neurons by minimizing the activity of these neurons until they receive massive coincident synaptic input, which reduces the periodic fluctuations of inspiratory activity.

(Resubmitted 10 January 2008; accepted after revision 5 February 2008; first published online 7 February 2008)
Corresponding author C. A. Del Negro: Department of Applied Science, McGlothlin-Street Hall, Room 318, The College of William and Mary, Williamsburg, VA 23187-8795, USA. Email: cadeln@wm.edu

Rhythmic motor behaviours originate from central pattern generator (CPG) networks in the brainstem and spinal cord (Marder, 2001). A key issue is to what degree proper network function (i.e. rhythmogenesis) depends on specific ion channels in constituent rhythm-generating neurons (Stein, 1997). The respiratory CPG is an excellent model for examining this question because its constituent rhythmogenic neurons are contained within the preBötzinger complex (preBötC) (Smith *et al.* 1991; Feldman & Del Negro, 2006) and the network output is measurable *in vitro*. Transverse medullary slices containing the preBötC spontaneously generate behaviourally relevant motor activity that can be monitored via the hypoglossal nerve (XII).

Most studies of respiratory rhythm generation have focused on the role of voltage-dependent inward currents (Mironov & Richter, 1998; Pierrefiche *et al.* 1999; Mironov *et al.* 2000; Thoby-Brisson *et al.* 2000; Del Negro *et al.* 2001, 2002*a*,*b*, 2005; Onimaru *et al.* 2003; Pena *et al.* 2004; Ptak *et al.* 2005; Pace *et al.* 2007*b*), neuromodulation (Johnson *et al.* 1996; Rekling *et al.* 1996*b*; Onimaru *et al.* 1998; Shao & Feldman, 2000; Pena & Ramirez, 2002, 2004; Ruangkittisakul *et al.* 2006), as well as excitatory and inhibitory synaptic currents (Greer *et al.* 1991; Funk *et al.* 1993, 1995; Brockhaus & Ballanyi, 1998; Pierrefiche *et al.* 1998; Shao *et al.* 2003; Paarmann *et al.* 2005; Pace *et al.* 2007*a*). Apart from an ATP-inhibited K^+ current primarily activated during hypoxia (Pierrefiche *et al.* 1996; Mironov *et al.* 1998, 1999; Mironov & Richter, 2000, 2001; Haller *et al.* 2001*a*,*b*), K^+ currents have not been well-characterized in the preBötC of neonatal rodents, nor have their contributions to rhythmogenesis been analysed.

Transient K^+ currents are important in invertebrate CPGs and the primitive vertebrate lamprey CPG for swimming, where they control the sequence of cell activation during the behavioural patterns and influence spike timing and frequency (Getting, 1983; Tierney & Harris-Warrick, 1992; Hess & El Manira, 2001).

 DOI: 10.1113/jphysiol.2008.150946

In the respiratory CPG, Rekling *et al.* (1996*a*) described a subset of inspiratory neurons that depolarized with a ramp-like trajectory and started spiking ∼400 ms prior to XII output, dubbed *type 1* neurons, which are putatively rhythmogenic (Rekling & Feldman, 1998; Gray *et al.* 1999). Type 1 neurons held at hyperpolarized membrane potentials exhibited delayed excitation in response to 400 ms step pulses of depolarizing current (Rekling & Feldman, 1998). Delayed excitation is often attributed to transient K^+ currents (i.e. A-currents, I_A) (Hagiwara *et al.* 1961; Getting, 1983; Dekin & Getting, 1987; Dekin *et al.* 1987; Nisenbaum *et al.* 1994), thus Rekling and colleagues proposed that rhythmogenic preBötC neurons expressed I_A, although they did not measure it in voltage clamp nor speculate on its role in rhythm generation (Rekling *et al.* 1996*a*; Rekling & Feldman, 1998). Inyushkin (2005) confirmed that preBötC neurons expressed I_A using voltage clamp, but stopped short of analysing its contributions to rhythmogenesis.

Here we studied preBötC neurons that became active preceding inspiratory bursts, which we refer to as 'early inspiratory' to distinguish them from more rostral 'pre-inspiratory' neurons (Onimaru *et al.* 2006), and sought to measure I_A and evaluate its role in rhythm generation.

Methods

The Institutional Animal Care and Use Committee at The College of William and Mary approved all protocols. Neonatal (P0–7) C57BL/6 mice were anaesthetized via hypothermia until mice lacked a tail-pinch response. Mice were rapidly decerebrated and then dissected. Transverse slices (550 μm thick) containing the preBötC and hypoglossal (XII) nerves were sectioned with a vibrating microtome from the medulla oblongata. The rostral cut captured the rostral-most XII nerves, the dorso-medial cell column and principal lateral loop of the inferior olivary nucleus while the caudal cut captured the obex.

Slices were perfused at 26–28°C with an artificial cerebrospinal fluid (ACSF) containing (mM): 124 NaCl, 9 KCl, 0.5 NaH_2PO_4, 25 $NaHCO_3$, 30 D-glucose, 1.5 $CaCl_2.2H_2O$, and 1 $MgSO_4$. We identified putatively rhythmogenic inspiratory preBötC neurons (see first section in Results, below) with 9 mM K^+ in the ACSF to maintain rhythmic network function, and then switched to 3 mM K^+ to isolate and measure the properties of I_A because the lower $[K^+]$ more closely matches the *in vivo* milieu. We acquired data from a total of 65 inspiratory neurons, 8 expiratory neurons, and 4 field-recordings in a total of 77 slices and 77 animals.

Most voltage- and current-clamp experiments were performed with a HEKA EPC-10 patch-clamp amplifier and Patchmaster software (Lambrecht, Germany). Dose–response experiments were performed with a Model 2400 patch-clamp amplifier (A-M Systems, Sequim, WA, USA) using Chart 5 software and a Powerlab 8/30 (AD Instruments, Colorado Springs, CO, USA) for stimulation. The remaining voltage-clamp experiments utilized a LabJack U3 (LabJack Corporation, Lakewood, CO, USA) as a waveform generator commanding the voltage-clamp amplifier controlled with custom C/C^{++} software written for a G4 Powerbook (Apple Inc., Cupertino, CA, USA). Respiratory-related motor output was monitored from XII nerves with extracellular suction electrodes and a high-gain differential amplifier with band-pass filtering (0.3–1 kHz) (Dagan Instruments, Minneapolis, MN, USA). Raw XII activity was conditioned using a true RMS-to-DC converter (Analog Devices, One Technology Way, Norwood, MA, USA) to provide a full-wave rectified and smoothed XII waveform. Data were acquired digitally and analysed using Chart 5, Igor Pro 5 (WaveMetrics, Lake Oswego, OR, USA), Excel (Microsoft, Redmond, WA, USA) and custom software. An 8 mV liquid junction potential was corrected online in both current- and voltage clamp.

Whole-cell capacitance (C_M) was measured using 50 ms voltage steps from −60 mV to command potentials from −75 mV to −65 mV in a 10-step sequence. Charge (Q) was computed by integrating leak-subtracted capacitative current ($\Delta Q = \int I_C$) and C_M was calculated from $C_M = \Delta Q/\Delta V$. Series (access) resistance (R_S) was monitored throughout voltage-clamp recordings according to the Thevenin equivalent circuit, which allows R_S to be calculated from the decay time constant (τ_m) in response to small voltage steps with $R_S = \tau_m/C_M$ as long as R_S was much less than the input resistance (R_N). We monitored R_N via P/N online leak protocols. To avoid voltage-clamp errors we discarded experiments in which $R_S > 0.1\ R_N$. We compensated for R_S in whole-cell using analog feedback circuitry within the EPC-10 as much as possible without causing clamp oscillations that jeopardize stable recording. We rechecked R_S and R_N to assess voltage-clamp viability before running sequences of episodic protocols, ensuring the reliability of the acquired data.

We used the following standard patch solution containing (mM): 140 potassium gluconate, 5 NaCl, 0.1 EGTA, 10 Hepes, 2 Mg-ATP, and 0.3 Na(3)-GTP. KOH was used to equilibrate pH at 7.2. To isolate I_A in voltage clamp (Figs 1*B*, 2*B*, 3, 5 and 7*A*) and test for delayed excitation as in Figs 1*C* and 2*C*, we used a low Ca^{2+}–high Mg^{2+} extracellular ACSF containing (mM): 124 NaCl, 3 KCl, 25 $NaHCO_3$, 30 D-glucose, 0.5 $CaCl_2{\cdot}2H_2O$, 2 $MgSO_4$, 0.001 TTX, and 0.2 $CdCl_2$.

We measured the voltage dependence and kinetics of I_A using Fitmaster software by HEKA (Lambrecht, Germany) and Igor Pro. Activation and inactivation functions took

the form:

$$x_\infty(V) = \frac{1}{1 + e^{(-\frac{(V-\theta_x)}{\sigma_x})}},$$

where x_∞ reflects voltage-dependent steady-state activation (m_∞) or inactivation (h_∞), θ_x is the membrane potential of half-activation (θ_m) or half-inactivation (θ_h), and σ_x is the slope factor.

We computed the time course of I_A using recorded voltage trajectories from current clamp (Fig. 6) and the chord conductance equation $I_A = g_A\, m_{A(\infty)}\, h_A\, (V - E_K)$. E_K was −71 mV to simulate *in vitro* conditions, the voltage-dependent parameters matched the values from Results, and $dh_A/dt = (h_{A(\infty)} - h_A)/\tau_h(V)$, with $\tau_h(V) = (202–0.42 \cdot V)$ (fitted empirically, see Fig. 5*B*). The differential equation was integrated using the 4th order Runge–Kutta method in custom C/C^{++} software run on Apple Macintosh G5 computers under OS 10.4. Integration step size was 0.25 ms to match the 4 kHz experimental sampling rate.

Inspiratory drive potentials were analysed using the Peak Parameters extension in Chart software. Leading and trailing slopes of the drive potential were calculated from digitally smoothed traces that minimize spikes but preserve the underlying drive potential characteristics (Pace *et al.* 2007*b*). Peak amplitude and baseline were automatically detected and the leading slope was computed from 20% of peak amplitude to 80% peak amplitude and trailing slope is calculated from 80% to 20%. Cycle-triggered averages were generated with custom software written in the Python programming language.

Sample means were generally compared using *t* test, or Fisher Exact test where indicated. Mean values are reported with standard error (mean ± S.E.M.) and significance was set at a *P* value of 0.05.

Results

Inspiratory preBötC neurons express I_A

Rhythmogenic neurons can be distinguished on the basis of small soma size (measurable via C_M) and an incremental pattern of depolarization followed by repetitive spike discharge several hundred milliseconds prior to inspiratory-related XII (or C4) motor activity (Fig. 1*A*) (Bianchi *et al.* 1995; Rekling *et al.* 1996*a*; Rekling & Feldman, 1998; Ballanyi *et al.* 1999; Richter & Spyer, 2001). In a prior study we showed that these intrinsic properties are a reliable means to identify rhythmogenic preBötC neurons (Hayes & Del Negro, 2007).

We isolated K^+ currents in whole-cell voltage clamp using low Ca^{2+} ACSF containing 3 mM extracellular [K^+], 1 μM TTX and 200 μM Cd^{2+}. Depolarizing step

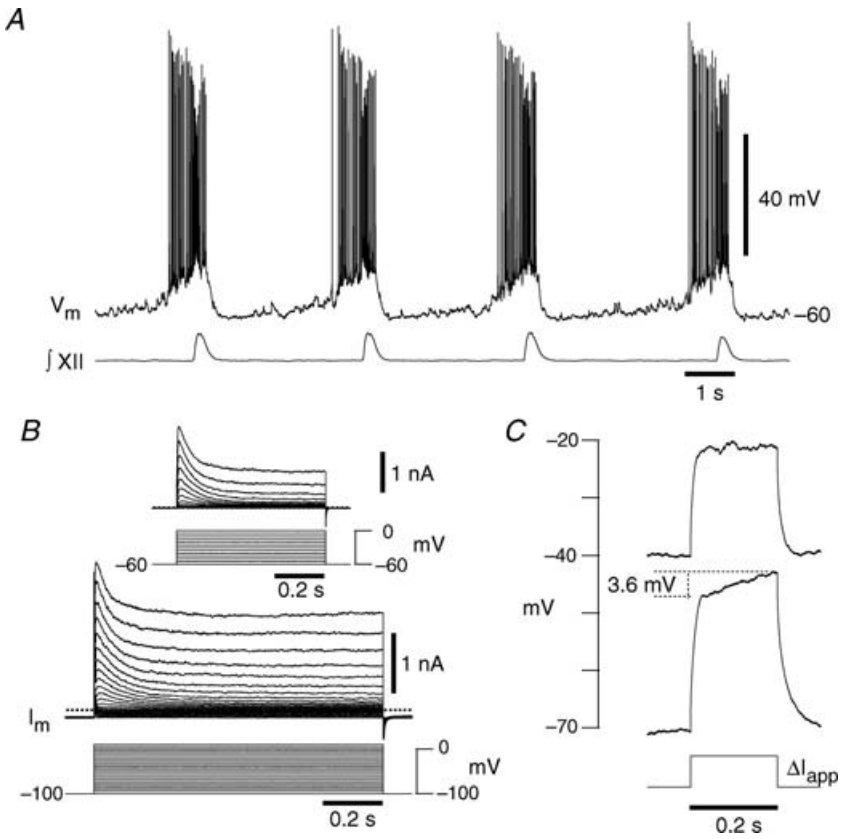

Figure 1. Phenotypic behaviours of inspiratory neurons located in the preBötC
A, current-clamp recording showing early inspiratory activity that precedes the integrated XII nerve (∫XII) output in 9 mM $[K^+]_o$, a hallmark property of rhythmogenic neurons. *B*, voltage-clamp recording from a holding potential of −100 mV illustrating the transient K^+ currents evoked at depolarized membrane potentials. Inset, a different neuron showing transient K^+ currents evoked from a holding potential of −60 mV. *C*, the same neuron as in *A* and *B* illustrating voltage-dependent delayed excitation where ΔI_{app} was 95 pA.

commands from −100 mV (up to +10 mV) evoked sustained K^+ currents in addition to transient K^+ currents, i.e. I_A (Fig. 1*B*). I_A could also be evoked by depolarizing step commands from a −60 mV holding potential (Fig. 1*B*, inset), suggesting that I_A does not completely inactivate at baseline membrane potentials observed during normal inspiratory activity *in vitro* (e.g. Fig. 1*A*).

In current clamp, depolarizing current steps from a holding potential of −70 mV evoked a ramping depolarization ($\Delta V/\Delta t = 18$ mV s^{-1}), whereas steps from −40 mV resulted in passive responses that quickly achieved steady state (Fig. 1*C*), which indicates that I_A is de-inactivated at hyperpolarized potentials, but steady-state inactivated at voltages above spike threshold.

Expiratory neurons in the preBötC are inhibited during XII motor activity but otherwise spike tonically (Fig. 2*A*). Their K^+ currents were typically smaller overall, and only one expressed I_A (compare Figs 1*B* and 2*B*, note scale bars are the same, $n = 8$). In current clamp, depolarizing step commands did not generally evoke a ramping depolarization from any holding potential (Fig. 2*C*), which is consistent with the lack of I_A.

Biophysical properties of I_A

We separated I_A from non-inactivating K^+ currents by subtraction. Using the same conditions as Figs 1*B* and 2*B*, we applied a sequence of 1 s step commands from −70 to +10 mV from a holding potential of −100 mV (Fig. 3*A*) and then repeated these steps from −40 mV (Fig. 3*B*). The difference current was defined as I_A, which activated at −60 mV and its maximum amplitude exceeded 1 nA at voltages greater than 0 mV (Fig. 3*C*).

Twenty-one of 34 (61.7%) inspiratory neurons expressed a peak transient outward current that exceeded the steady-state outward current and decayed exponentially with a time constant greater than 15 ms, which we defined as measurable I_A (Fig. 4*A*). This fraction of expression was significantly different from the 1/8 (12.5%) expiratory neurons found to express I_A (Fisher Exact test: $P = 0.015$).

For inspiratory neurons expressing I_A, C_M measured 53.6 ± 5.9 pF ($n = 21$) and the difference between the onset of inspiratory-related EPSPs and the upstroke of XII activity (i.e. the *drive latency*) measured 305.2 ± 14.7 ms, which suggests these cells are putatively rhythmogenic (Rekling *et al.* 1996*a*; Rekling & Feldman, 1998; Feldman & Del Negro, 2006; Hayes & Del Negro, 2007). The C_M of neurons expressing I_A was directly related to g_A (Fig. 4*B*). Fitting the whole-cell conductance for I_A (g_A) linearly with C_M, with a *y*-intercept at zero, resulted in a slope of 0.219 ± 0.09 nS pF^{-1}. There was no obvious relationship between R_N of neurons expressing I_A and g_A (Fig. 4*C*).

The 13 of 34 (38.2%) preBötC neurons without measurable I_A exhibited drive latencies of 321.7 ± 14.6 ms and C_M of 44.4 ± 3.1 pF, which were indistinguishable from I_A-expressing neurons (latencies: $P = 0.428$; C_M: $P = 0.181$). Histograms of drive latencies for neurons with and without I_A are depicted in Fig. 4*D* showing the substantial overlap of the variability of burst activation. The g_A for neurons with I_A tends to increase as the drive latency decreases (Fig. 4*E*, latency = –0.008 g_A + 13.6).

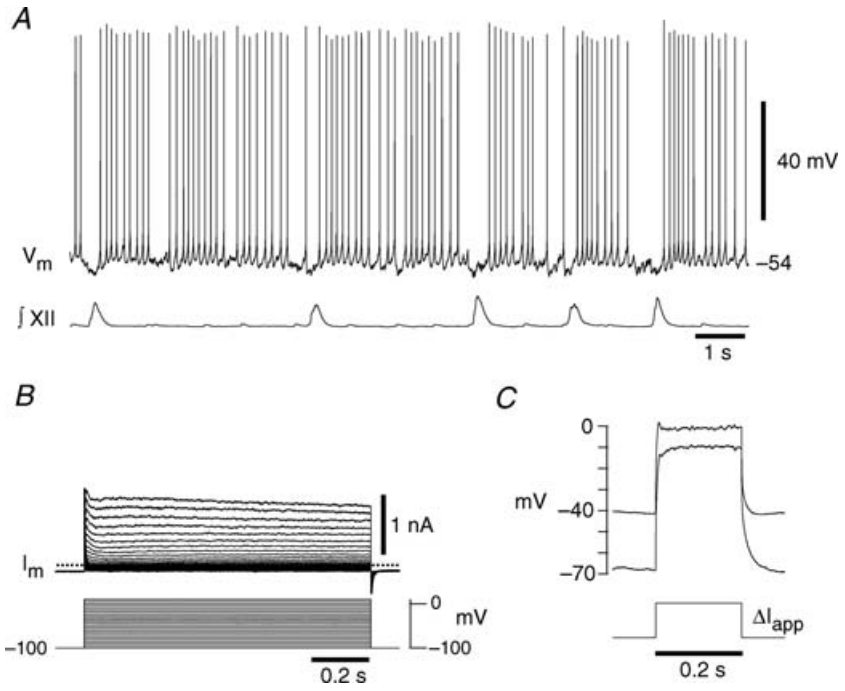

Figure 2. Phenotypic behaviours of expiratory neurons located in the preBötC
A, current clamp showing tonic spiking during the expiratory phase that is inhibited during ∫XII output in 9 mM $[K^+]_o$, a hallmark property of expiratory neurons. *B*, the corresponding voltage-clamp recording shows only minimal transient K^+ currents. *C*, delayed excitation is not exhibited by the expiratory neuron where ΔI_{app} was 379 pA.

Cycle-triggered averages (Fig. 4*F*) indicate that in neurons with I_A ($n = 16$) the voltage trajectory prior to the inspiratory phase shows a more abrupt rise that is statistically different from neurons without I_A ($n = 8$) (79.1 ± 11.6 ms *versus* 120.4 ± 14.4 ms, $P = 0.037$).

Detailed voltage-clamp analysis was precluded in whole-cell recordings because of inherent space-clamp limitations and series resistance errors attributable to large magnitude membrane currents (Armstrong *et al.* 1992). Therefore we studied I_A in somatic outside-out patches, repeating the subtraction protocol described above with step commands that reached +30 mV (Fig. 5*A*). The I_A activation function (see Methods) was fitted with the parameters $\theta_m = -16.3$ mV and $\sigma_m = 14.9$ mV. Even in patches, I_A generally exceeded 200 pA with a maximum conductance of 1.14 ± 0.36 nS ($n = 6$).

We measured the steady-state inactivation of I_A at +10 mV for 500 ms following 1 s conditioning prepulses from −100 to +10 mV. The inactivation curve reaches its minimum above −40 mV and was fitted with the parameters $\theta_h = -85.6$ mV and $\sigma_h = -13.8$ mV. These data explain why transient K^+ currents can be evoked from a holding potential of −60 mV (e.g. Fig. 1*B*, inset); I_A is not fully inactivated at that potential, $h_\infty(-60) = 0.135$ (Fig. 5*B*).

Over the range −30 to +30 mV, the inactivation time constant for I_A was 200–300 ms and could be empirically fitted with a line in the form, $\tau_h(V) = 202–0.42\,V$ (Fig. 5*B*, bottom). Interestingly, $\tau_h(V)$ of ∼200 ms is commensurate with both the ramping depolarization responses observed in current clamp from baseline voltages of −70 mV (e.g. Fig.1*C*) and the transient ramp-like depolarization seen during endogenous network activity (e.g. Fig. 1*A*), suggesting the involvement of I_A in these membrane behaviours.

We computed the expected time course of I_A for the neuron in Fig. 1*A* to ascertain if and when the current would be active during the respiratory cycle (Fig. 6*A*). We used g_A of 11.7 nS, commensurate with the average maximum conductance, the chord conductance equation $I_A = g_A{}^* m_{A(\infty)}{}^* h_A{}^* (V - E_K)$, the equation for inactivation gating (dh_A/dt), and empirically determined voltage dependence and kinetics (i.e. Fig. 5*B*). As the neuron begins to initiate the inspiratory burst, I_A rapidly achieves ∼60 pA, then diminishes throughout the burst and measures ∼40 pA at burst termination (Fig. 6*B*). This illustrates that I_A provides hyperpolarizing current during the burst with a particularly large influence at burst onset.

I_A exhibits window current between −60 and −40 mV that peaks at −52.2 mV with 0.6% of the maximum current active at steady state. This suggests that I_A does not substantially influence the baseline membrane potential during the majority of the quiescent phase of network activity but nonetheless resides in a sufficiently de-inactivated state that it can be rapidly evoked by depolarization; $h_{A(\infty)}$ is less than 0.2 through the expiratory phase (Fig. 6*C*). This is supported by the simulation where only 1–2 pA of I_A flows during the inter-inspiratory burst interval, yet I_A rapidly exceeds 50 pA at burst onset (Fig. 6*B*). Since voltage-clamp measurements may be subject to error, we examined whether disparities in the activation and inactivation curves could influence I_A. We

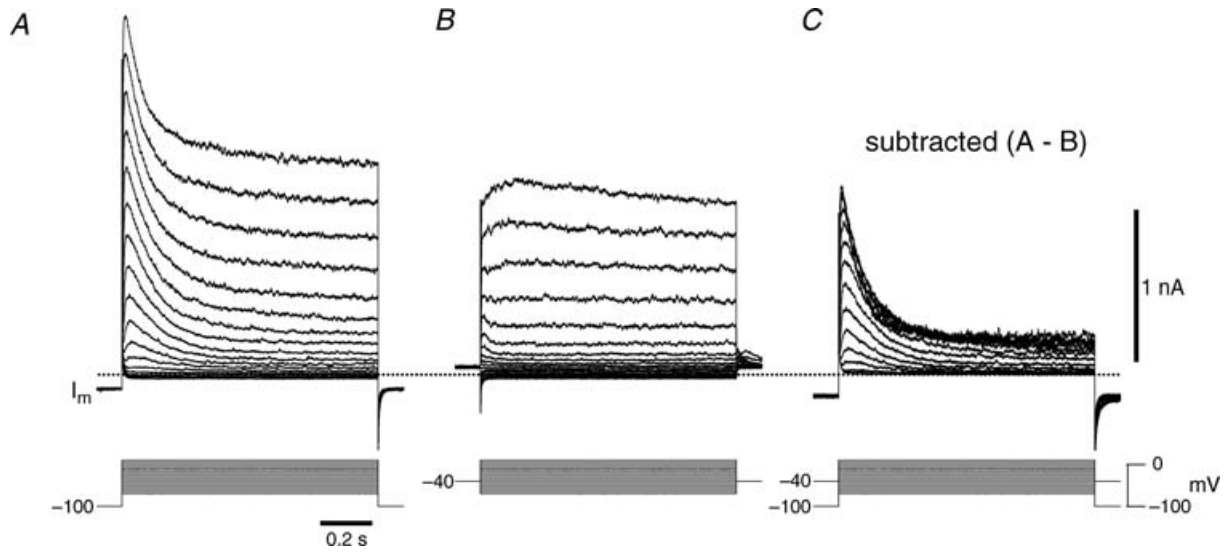

Figure 3. Isolation of I_A in inspiratory neurons
A, voltage-clamp recording from a holding potential of −100 mV illustrating the transient K^+ currents evoked at depolarized membrane potentials. *B*, voltage-clamp recording from a holding potential of −40 mV illustrating the lack of significant transient K^+ currents evoked at depolarized membrane potentials. *C*, I_A was isolated by subtracting the current traces in *B* from *A* while the voltage-clamp protocols are shown superimposed.

shifted the half-activation and half-inactivation 10 mV in both the positive and negative direction and re-ran the simulations. When both curves were shifted, peak current was linearly related to the magnitude of the shift with a 60% increase for a +10 mV shift and a 42% decrease for a −10 mV shift, while the time course of I_A did not change. Regardless of shifts in voltage dependence, less than 2 pA of I_A flowed during the inter-inspiratory burst interval. These data suggest that I_A may play a role in inspiratory burst dynamics primarily as a result of the large conductance and its availability for activation, but I_A has little influence during the interburst membrane trajectory.

To test the role of I_A in the preBötC we first had to understand its pharmacology. We performed dose–response experiments with 4-aminopyridine (4-AP) in outside-out patches (Fig. 7*B*, $n = 13$). We measured the change in peak transient outward current due to 4-AP and the change in the total area of the transient outward component. The IC_{50} for the peak response was 2.0 mM, which is close to the IC_{50} of most A-currents (Rogawski, 1985). The IC_{50} for the total area was 0.8 mM, while approximately 20% of the transient outward current could not be blocked by even saturating doses of 4-AP.

4-AP (2 mM) substantially attenuated I_A in outside-out patches (Fig. 7*A*); 4-AP likewise attenuated I_A in whole-cell recordings ($n = 4$), as previously shown (Inyushkin, 2005). Interestingly, non-inactivating outward currents evoked from the holding potential −40 mV were unaffected by 4-AP. We computed the 4-AP-sensitive current not attributable to I_A by subtracting the current evoked at +30 mV (from a holding potential of −40 mV) in control and 4-AP conditions, which measured < 25 pA. In contrast, the 4-AP-sensitive I_A regularly exceeded 200 pA (Fig. 7*A*), where I_A was defined as the subtracted current at +30 mV following prepulse holding potentials of −100 mV and −40 mV (Fig. 3). These data indicate that 4-AP attenuates I_A but does not affect sustained outward currents at baseline membrane potentials

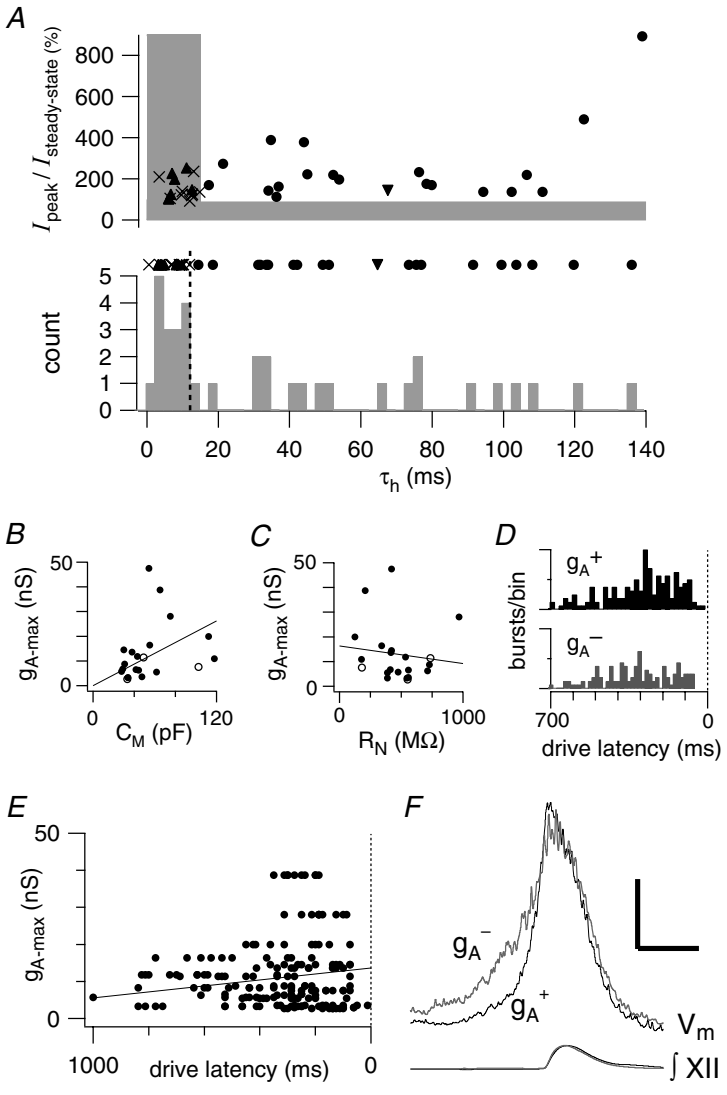

Figure 4. Whole-cell characteristics of I_A in preBötC neurons
A (top), the peak transient current normalized to the steady-state outward current plotted *versus* the measured whole-cell time constant of inactivation of outward currents (τ_h). The shaded area represents the boundary of measurements that were classified as not expressing I_A. Filled circles represent measured I_A-expressing inspiratory neurons, the downward pointed triangle represents the single I_A-expressing expiratory neuron, the crosses represent the inspiratory neurons that did not express I_A, and the upward pointing triangles represent non-I_A-expressing expiratory neurons. *A* (middle), the data points from top panel collapsed onto the τ_h axis. *A* (bottom), a histogram of the samples from middle panel in 2.5 ms bins. Points to the right of the vertical dashed line were called I_A-expressing neurons. *B*, the measured maximum conductance of I_A ($g_{A\text{-}max}$) *versus* C_M. The diagonal line represents a fit to the data with the *y*-intercept at the origin. Filled circles represent data points acquired using the subtraction protocol described in the text, while open circles represent data points acquired from a holding potential of −60 mV which may underestimate $g_{A\text{-}max}$. *C*, the $g_{A\text{-}max}$ *versus* R_N where the diagonal line is a linear fit to the data with no constraints. *D*, a pooled histogram showing the drive latencies of inspiratory neurons that expressed I_A (g_A^+) or did not not (g_A^-) with up to 10 cycles per neuron. The maximum ordinate on each histogram is 16 bursts bin^{-1}. *E*, the drive latencies from each neuron with a given g_A. The line is fitted to the mean drive latencies of the pool of neurons. *F*, cycle-triggered averages of the membrane trajectory of inspiratory neurons with their associated XII recorded below. The vertical scale bar is 5 mV while the horizontal scale bar is 400 ms.

(e.g. channels related to the KCNQ subfamily). Consistent with blockade of I_A, delayed excitation in whole-cell current clamp, evoked by 500 ms current steps in the interval between XII discharge from a holding potential less than −70 mV, was also abolished by 4-AP (Fig. 7*C*). We also analysed the effects of 4-AP on pulse-evoked spikes (Fig. 7*D*). In 189 spikes of 4 neurons tested at rheobase, 2 mM 4-AP significantly increased the width at half-maximum of spikes 177 ± 26% from 2.7 ± 0.1 to 4.8 ± 0.6 ms ($P = 0.031$) and the area of the spike to 137 ± 13% from 304.7 ± 18.8 to 416.9 ± 23.2 mV·ms ($P = 0.023$). Some of this effect may have been attributable to attenuation of I_A (see simulated time-course and magnitude of I_A in Fig. 7*D*), but is more likely due to 4-AP effects on other channels in the Kv subfamily, which give rise to currents with delayed rectifier-like properties in addition to I_A.

Since I_A is expressed in more than half of the inspiratory preBötC neurons we recorded, in which it is available at typical baseline membrane potentials and generates large magnitude outward currents lasting several hundred milliseconds (Figs 1 and 3–7), we posited that I_A could influence rhythmogenesis.

4-AP affects rhythmic activity in the preBötC

We used 4-AP sensitivity to test the role of I_A in rhythm generation. In the context of respiratory network activity 4-AP caused erratic XII output that could not be straightforwardly interpreted. Therefore, we sought to determine whether the disorganized XII activity reflected a breakdown in rhythmogenesis by performing field recordings within the preBötC while recording the contralateral XII activity (Fig. 8*B*). The preBötC and XII activity patterns were coherent and recognizably rhythmic in control and washout, whereas 4-AP caused noisy preBötC rhythms that fluctuated in amplitude and period, and did not always match the output of the XII channel (Fig. 8*A*, $n = 4$). Under these conditions, the average rise time of the inspiratory activity within the preBötC decreased significantly in the presence of 4-AP from 141.3 ± 5.14 to 86.3 ± 8.8 ms ($P = 0.016$), while the falling slope did not change ($P = 0.760$, Fig. 8*C*).

As 4-AP perturbed rhythmic activity in preBötC field recordings we sought to determine the cellular basis for population-level fluctuations via whole-cell recordings and analyses (Figs 9 and 10).

The depolarizing activity occurring 400 ms (or more) prior to the inspiratory burst is largely synaptically driven, as we showed previously (Hayes & Del Negro, 2007). This early inspiratory activity can be observed in the on-cell recording configuration prior to whole-cell (Fig. 9*A*). In current clamp at baseline membrane potential (approximately −60 mV) the ascending ramp-like trajectory is accompanied by vigorous spiking. Hyperpolarizing the membrane potential reveals the temporal summation of EPSPs in the early inspiratory phase, which are also well resolved as summating EPSCs in voltage clamp (Fig. 9*A*, left to right). These data emphasize that a rapidly activating K^+ current, which

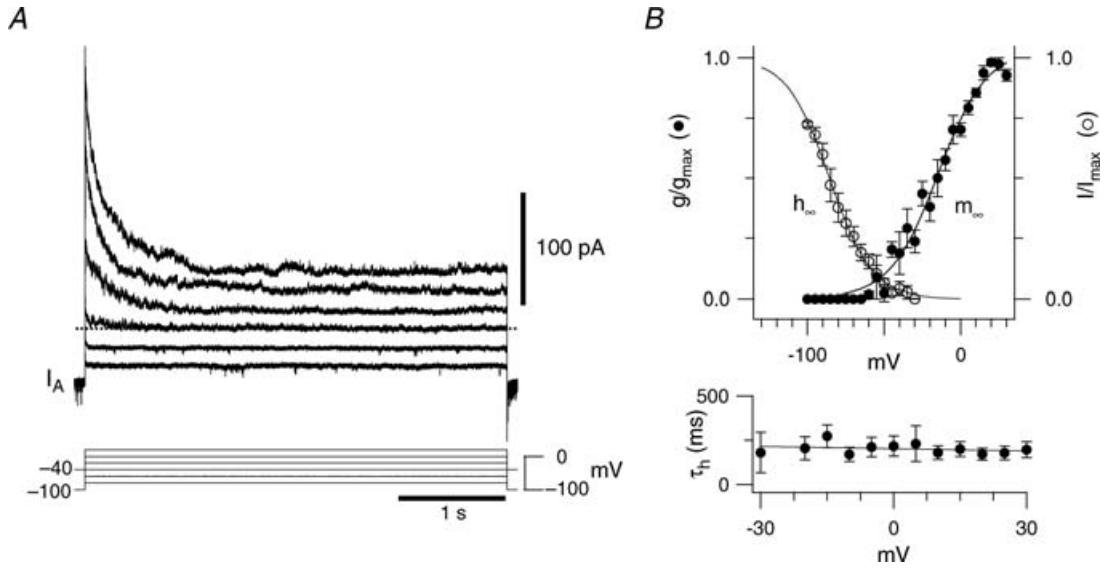

Figure 5. Biophysics of I_A in inspiratory neurons
A, the voltage dependence of activation measured from difference currents evoked by depolarizing step commands delivered from −100 mV and −40 mV in an outside-out patch. The voltage-clamp protocols are shown superimposed and alternating traces were eliminated to facilitate illustration. *B*, steady-state activation curve (m_∞) and inactivation curve (h_∞) from outside-out patches (top). The time constant of inactivation (τ_h) as a function of voltage (bottom).

is de-inactivated at baseline voltages and subject to temporally summating synaptic inputs, may be uniquely poised to influence the dynamics of the inspiratory burst pattern.

We tested this idea by applying 2 mM 4-AP and measuring its effects on inspiratory bursts (Fig. 9*B* and *C*). The pattern changed from incrementing in control to decrementing in the presence of 4-AP (Fig. 9*B*). The leading slope of the inspiratory burst changed significantly in 4-AP from 53.1 ± 7.4 to 80.2 ± 5.3 mV $\cdot$ s^{-1} ($P = 0.032$, $n = 8$, Fig. 9*C*). However, the trailing slope did not change significantly: -52.7 ± 2.5 mV s^{-1} in control *versus* -65.5 ± 6.0 mV s^{-1} in 4-AP ($P = 0.095$, $n = 8$, Fig. 9*C*). These general features are consistent with the average field-recording data analysed in Fig. 8*C*.

These data suggest that 4-AP removed a hyperpolarizing current that normally influenced the onset of the inspiratory burst, but its influence diminished during the inspiratory burst, which is consistent with the role of I_A we predicted (Fig. 6). Moreover, 4-AP did not change the baseline membrane (bias current is 0 pA in Figs 9*B* and 10*A*), which is consistent with the lack of significant window current measured in voltage clamp (see Fig. 5*B*) as well as the predictions of our simulation (Fig. 6*B*).

We also analysed the effect of 4-AP on drive potential amplitude and its coefficient of variation (CV) as well as respiratory cycle period and its CV. A representative experiment illustrates that burst sizes became more variable and that the timing of the neuronal activity became more variable (Fig. 10*A*). We applied a 5 Hz low-pass filter to the voltage trajectory, which filters out spikes and facilitates measurements of the underlying inspiratory drive potentials (Pace *et al.* 2007*b*). The amplitude and period of inspiratory activity fluctuated in 4-AP. The average period of drive potentials did not change significantly between control and 4-AP application ($P = 0.052$) while the CV for period approximately doubled from 0.32 ± 0.05 to 0.52 ± 0.03, which was statistically significant ($P = 0.006$, $n = 8$, Fig. 10*B*). The average amplitude of the drive potential did not significantly change ($P = 0.408$) but the CV for amplitude changed significantly from 0.26 ± 0.06 to 0.58 0.08 ($P = 0.015$, $n = 8$, Fig. 10*C*), which suggests that I_A influences the regularity of both the cycle period and the drive potential magnitude in preBötC neurons.

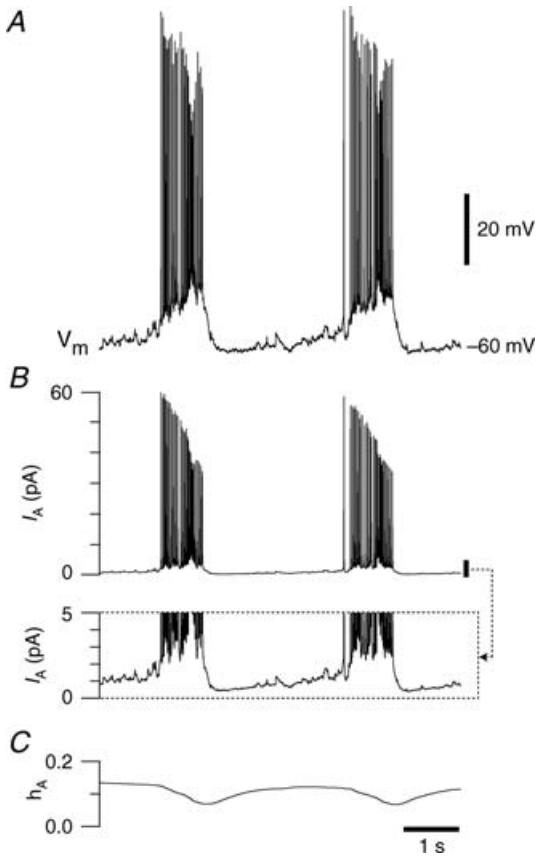

Figure 6. Simulating the role of I_A
A, the membrane trajectory from Fig. 1*A*. *B*, the time course of I_A as computed from Hodgkin–Huxley-style equations (see Methods). Inset, a detail of the calculated I_A with expanded *y*-axis emphasizing the low magnitude (1–2 pA) of the current during the interburst interval. *C*, the time course of the computed h_A.

Discussion

We studied biophysical properties of I_A in preBötC neurons and analysed its role in respiratory rhythm generation. I_A recovers from inactivation at membrane potentials traversed during the interburst interval and remains relatively de-inactivated at baseline voltages, and thus available to be readily activated at the onset of the inspiratory phase of each respiratory cycle. I_A is prevalent among inspiratory neurons while being sparse in expiratory neurons. We found that inspiratory neurons expressing I_A received synaptic input at approximately the same time on average as inspiratory neurons that lack significant I_A (Fig. 4*D*), but that the rate at which these neurons responded to network activity was slower (Fig. 4*E*). Blockade of I_A increased the rate at which peak activity was achieved at both the network (Fig. 8*C*) and neuronal level (Fig. 9) which was correlated with an increase in the variability of both burst amplitude and period. Our data suggest that I_A may normally slow the onset of network inspiratory activity by counteracting excitatory synaptic input until there is massive excitatory drive to overcome I_A. We suggest this thereby promotes regular burst size and frequency throughout the network by suppressing spurious inputs.

The rhythm and pattern for breathing are generated in the brainstem. Neurons in the dorsal respiratory group (DRG), including the nucleus tractus solitarius (NTS) where I_A has been characterized (Champagnat *et al.* 1986;

Dekin & Getting, 1987; Dekin *et al.* 1987), participate in afferent feedback and autonomic regulation. The ventral respiratory group (VRG) contains a bilaterally distributed column of neurons including rhythmogenic interneurons concentrated in the preBötC as well as premotoneurons that project to cranial and spinal motoneurons to carry out breathing movements (Bianchi *et al.* 1995; Onimaru *et al.* 1997; Ballanyi *et al.* 1999).

The role of I_A has been studied in mathematical models of respiratory networks that include the VRG and DRG, which predicted that I_A could influence the initial ramping trajectory of inspiratory neurons if it were sufficiently de-inactivated during the interburst phase of the respiratory cycle (Rybak *et al.* 1997). However, one caveat is that this network model did not explicitly consider the dynamics of preBötC neurons as a centre of rhythm generation and subsequent models of the preBötC have not analysed the role of I_A (Butera *et al.* 1999*a*,*b*; Del Negro *et al.* 2001; Rybak *et al.* 2003, 2004; Kosmidis *et al.* 2004). Our study is the first detailed characterization of I_A from putatively rhythmogenic preBötC neurons, as well as the first analysis of the role of I_A during endogenous respiratory network activity *in vitro*.

Role of I_A in the preBötC *in vitro*

We measured the voltage dependence and kinetics of I_A in somatic outside-out patches to minimize space-clamp limitations and series-resistance errors. I_A activates near −60 mV and is not fully inactivated until approximately −30 mV. Because these activation and inactivation functions encompass the range of membrane potentials visited during the interval between inspiratory bursts, I_A resides in a partially de-inactivated state at typical baseline membrane potentials *in vitro*. However, I_A has little window current, and consequently 4-AP

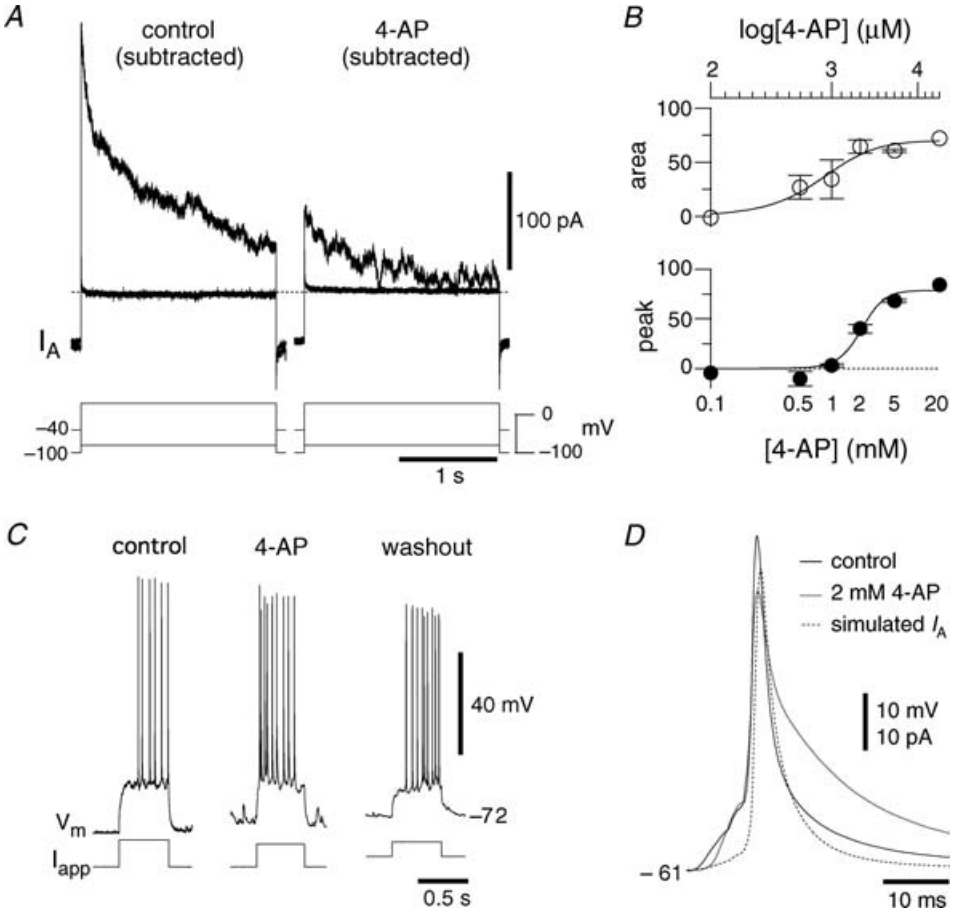

Figure 7. 4-Aminopyridine attenuates I_A and blocks delayed excitation
A, difference currents evoked from −100 and −40 mV in somatic outside-out patches in the presence of 1 μM TTX, 200 μM Cd^{2+} and 3 mM extracellular [K^+] before and after application of 2 mM 4-AP. Two activation steps are shown: −80 mV and +30 mV. *B*, dose–response curve of I_A in outside-out patches. *C*, in a different cell from *A*, 2 mM 4-AP abolished delayed excitation in current clamp. This neuron is also analysed in Fig. 9. *D*, the effects of 4-AP on pulse-induced spikes averaged over 4 neurons.

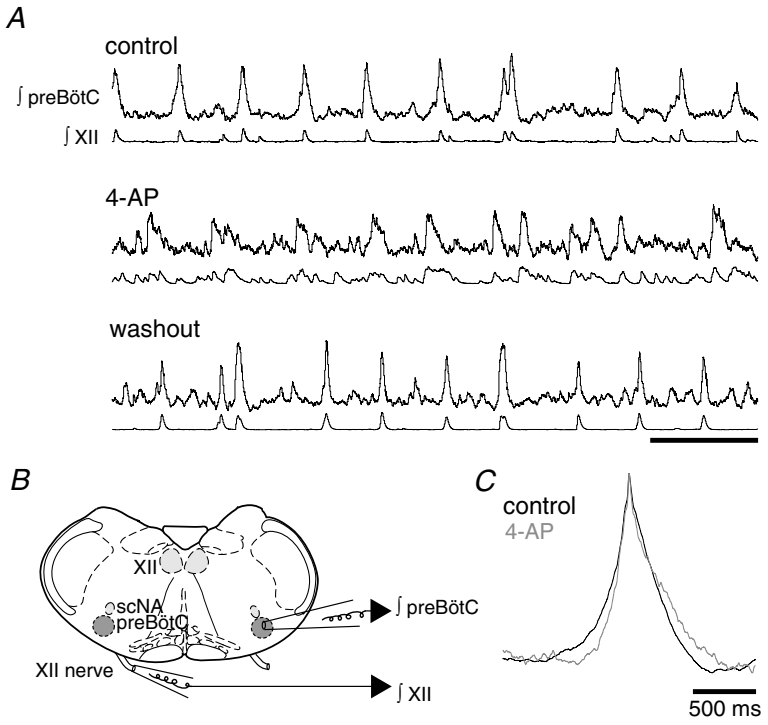

Figure 8. Effects of 4-AP on the preBötC network
A, ∫preBötC (top traces) and ∫XII (bottom traces) under control conditions, in the presence of 2 mM 4-AP and washout. Scale bar is 5 s. *B*, cartoon showing the configuration of the preBötC field-recording pipette (∫preBötC) and ∫XII suction electrode in *A* and *C*. The subcompact division of the nucleus ambiguus is indicated by scNA, and the hypoglossal motonucleus is indicated by XII. *C*, cycle-triggered averages of the field preBötC recordings under control conditions and in 2 mM 4-AP ($n = 4$).

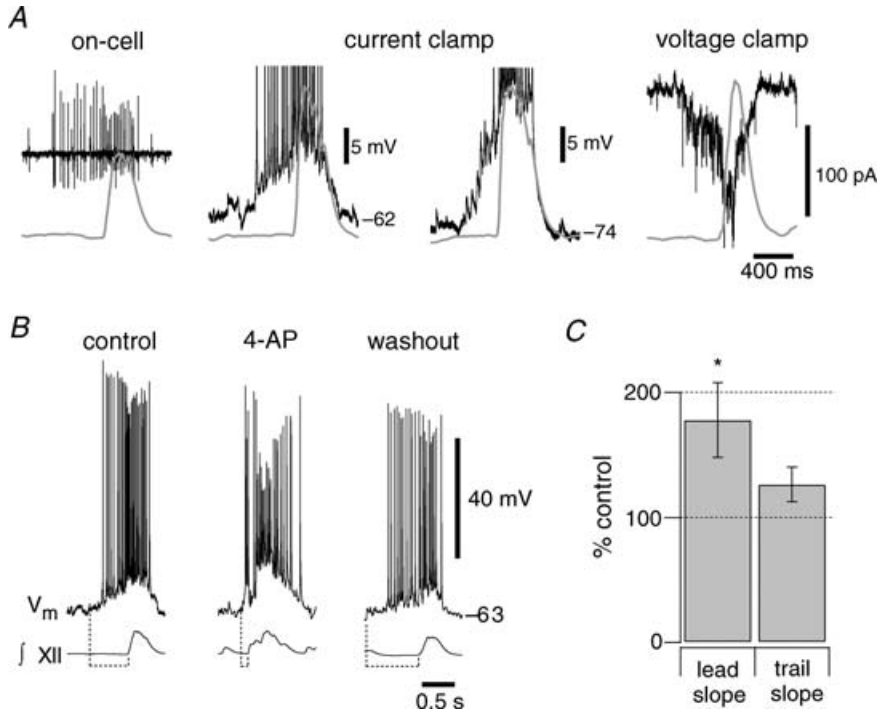

Figure 9. I_A affects the discharge pattern of preBötC neurons
A, on-cell activity of a preBötC neuron with early inspiratory spiking relative to the ∫XII. Current-clamp recording at 0 pA holding current illustrating similar activity as observed on-cell, i.e. early inspiratory spiking relative to XII output. Current-clamp recording at −40 pA holding current reveals temporal summation of EPSPs, beginning 400 ms prior to XII output. Voltage-clamp recording at a holding potential of −60 mV shows temporal summation of EPSCs prior to XII output. Baseline current was −25 pA. *B*, the burst discharge pattern changes from predominantly incremental (left) to decremental (middle) and back to incremental in washout (right). All recordings were at 0 pA bias current. Dashed lines at the bottom indicate the change in drive latency for each inspiratory burst illustrated. Traces in *A*, *B* and 7*C* were recorded in the same neuron. *C*, summary of the effects of 4-AP on the leading and trailing slope of inspiratory bursts ($n = 8$). Significance at $P < 0.05$ is shown with an asterisk.

application did not depolarize preBötC neurons. These properties indicate that I_A contributes little to the baseline membrane potential but can be rapidly recruited by synaptic depolarization at the onset of the inspiratory phase of the respiratory cycle (see Fig. 6).

I_A often causes delayed excitation, wherein the depolarization evoked by current pulses evolves with a ramp-like trajectory lasting several hundred milliseconds (or longer) because I_A activates rapidly and inactivates slowly (Hagiwara *et al.* 1961; Getting, 1983, 2989; Dekin & Getting, 1987; Gabel & Nisenbaum, 1998). Delayed excitation affects synaptic integration (Storm, 1988; Hoffman *et al.* 1997; Gulledge *et al.* 2005). This is particularly relevant in preBötC neurons with small C_M and early drive latency that are probably rhythmogenic, in which synaptic excitation builds up over several hundred milliseconds prior to respiratory-related motor output (Rekling *et al.* 1996*a*; Rekling & Feldman, 1998; also see Fig. 1*A* and 9; Hayes & Del Negro, 2007). Since I_A produces delayed excitation in preBötC neurons, is de-inactivated at baseline membrane potentials (Fig. 1*B* inset and 5*B*), and has a 200 ms inactivation time constant, we conclude that I_A plays a major role in shaping the ramp-like incremental discharge pattern characteristic of rhythmogenic neurons. Supporting evidence for this role is the dramatic increase in the leading slope of inspiratory activity following 4-AP application (Figs 8*C* and 9) as well as our comparison of membrane trajectories between neurons that express I_A and those that do not (Fig. 4*F*).

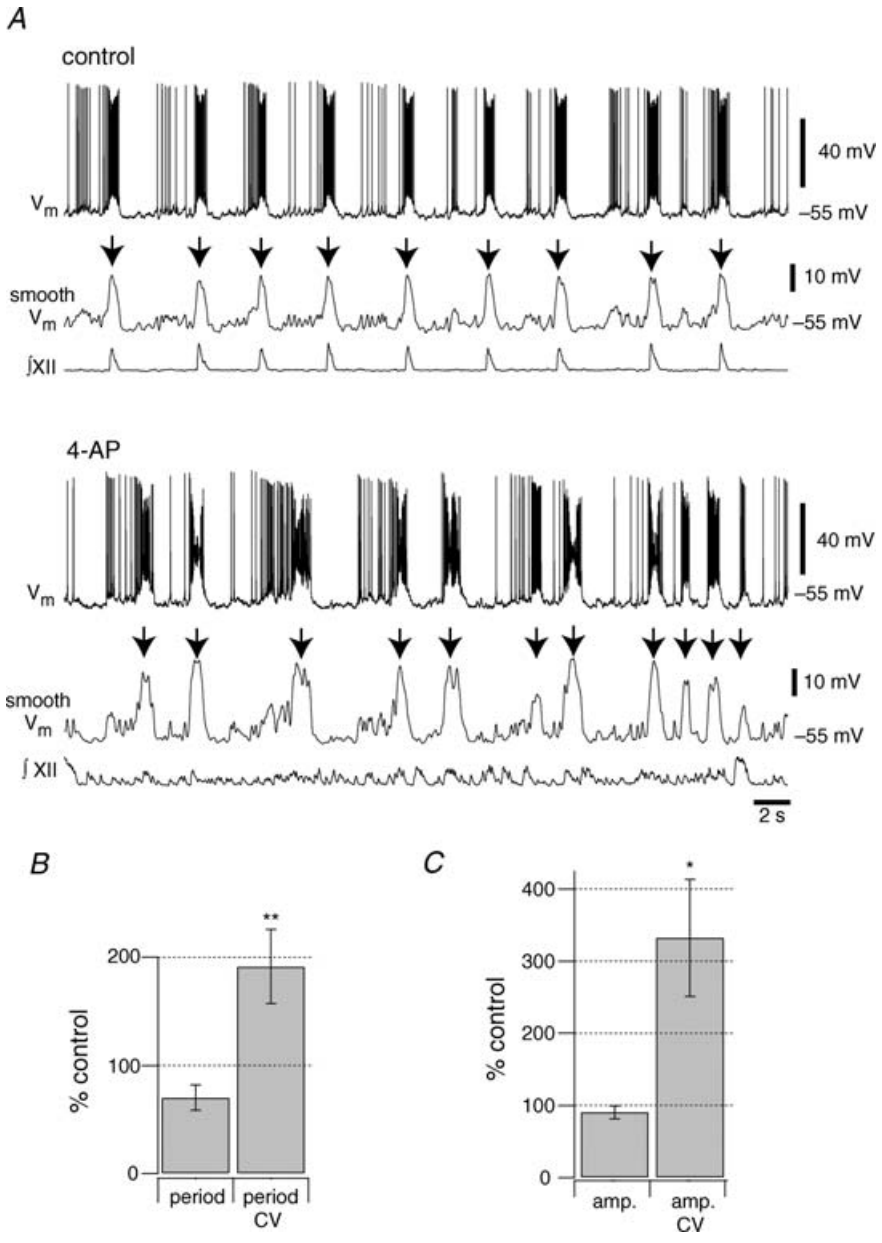

Figure 10. Effects of 4-AP on the period and amplitude of inspiratory bursts
A, current-clamp recordings of an inspiratory neuron in control and 2 mM 4-AP. All recordings were at 0 pA bias current. Smooth V_m denotes traces conditioned by a 5 Hz low-pass filter subsequently used to select inspiratory burst events (indicated by down arrows) and to measure their period and amplitude for the analyses in *B* and *C*. *B*, the mean change in burst period and coefficient of variation ($n = 8$). *C*, the mean change in burst amplitude and coefficient of variation ($n = 8$). Significance at $P < 0.05$ and $P < 0.01$ are shown with single and double asterisks, respectively.

In invertebrate CPGs, I_A regulates the order in which rhythmogenic neurons discharge (Getting, 1983; Tierney & Harris-Warrick, 1992). In the stomatogastric ganglion of lobster *Panulirus interruptus*, I_A slows the frequency of anterior burster and pyloric dilator cells and delays the response to inhibition of follower lateral, early, and late pyloric cells (Tierney & Harris-Warrick, 1992). Likewise in the opistobranch mollusk *Tritonia diomedea*, I_A causes the appropriate tail escape–swim pattern to be generated by delaying the activation of ventral swimming interneurons that receive synaptic input from cerebral cell 2 (Getting, 1983). Additionally, in the inking behavioural circuits of *Aplysia californica*, I_A impedes ink release in the absence of substantial synaptic input to L14 neurons (Byrne *et al.* 1979; Byrne, 1980).

In the mammalian preBötC, network rhythms continued in the presence of 4-AP and could be measured in whole-cell and field recordings. 4-AP did not affect the mean period or amplitude of inspiratory burst-like discharges, but it did significantly increase period and amplitude variability (Fig. 10*B* and *C*). The increase in variability was correlated with the diminished ramp-like incremental discharge pattern in 4-AP. One possible explanation for the destabilization of periodic preBötC activity is that, like in *Aplysia*, I_A delays neuronal activation until the temporal summation of excitatory synaptic input builds up sufficiently to overcome and outlast the transient K^+ current. We found that the more I_A is expressed in a neuron, the less the neuron is responsive to synaptic input preceding a burst (Fig. 4*E* and *F*) which is consistent with this hypothesis. However, the neurons lacking I_A are not expected to reach their peak activity until the neurons expressing some degree of I_A, which make up the majority of early inspiratory neurons, are also active. Thus I_A would influence the orderly recruitment of rhythm-generating neurons in the build-up to the inspiratory burst and ensure that the inspiratory phase does not begin until and unless a substantial fraction of the rhythmogenic population was involved. We speculate that this role for I_A would promote regularity in respiratory network behaviour, since the pharmacological attenuation of I_A caused substantial fluctuations in the amplitude and period of inspiratory burst activity.

An important caveat to this assertion is that 2 mM 4-AP extends spike duration significantly (Fig. 7*D*), which suggests that other outward currents may be affected by 4-AP such as Ca^{2+}-activated K^+ currents (Andreasen, 2002) or delayed-rectifier currents (Rusch & Eatock, 1996). However, the trailing slope of bursts did not change significantly at the network level (Fig. 8*C*) or neuronal level (Fig. 9*C*) suggesting the contribution of any outward currents active at the end of the burst were not significantly affected by 4-AP.

The above interpretation is further complicated by the fact that other neurons contained in slice preparations are also sensitive to 4-AP. Both raphé neurons (Aghajanian, 1985) and NTS neurons (Haddad & Getting, 1989) express I_A and project to preBötC neurons (Al-Zubaidy *et al.* 1996; Blessing, 1997; Pace *et al.* 2007*b*). These neurons may influence the preBötC by providing spurious excitatory or inhibitory input in 4-AP, but given that the slope of inspiratory activity changes in field recordings and in intracellular recordings, which is expected with a blockade of I_A, we are confident that at least some of this modulation is due to direct effects on rhythmogenic preBötC neurons. It is also unlikely that expiratory neurons in the preBötC that project to inspiratory cells can explain the effects of 4-AP on network activity because they did not express significant I_A.

Raphé and NTS neurons also project to hypoglossal motoneurons (Rekling *et al.* 2000). If these projection neurons are the same ones that have been shown to express I_A (Champagnat *et al.* 1986; Dekin & Getting, 1987; Dekin *et al.* 1987) then their response to 4-AP could further contribute to the very erratic XII discharge we observed. Evidence in support of this notion is that 4-AP is known to substantially increase spontaneous synaptic input to XII motoneurons and that I_A in XII motoneurons is relatively 4-AP-insensitive, fast-inactivating and mainly involved in spike repolarization (Haddad *et al.* 1990; Viana *et al.* 1993; Lape & Nistri, 1999).

Molecular identity of preBötC I_A

I_A in preBötC neurons shares similar voltage sensitivity and kinetic properties as members of the *Shal*-family (Kv4) K^+ channels (Pak *et al.* 1991). In particular, mammalian Kv4.1 and Kv4.3 channels expressed in *Xenopus* oocytes (Serodio *et al.* 1994, 1996) closely match the I_A that we recorded in the preBötC. Kv4.1 subunits are sparsely expressed in mammalian brain tissue while Kv4.3 is widespread (Trimmer & Rhodes, 2004) and has voltage-independent kinetics (Serodio *et al.* 1996). This suggests that Kv4.3 expression may give rise to at least some of the I_A in preBötC neurons. Kv4.2 is also a good candidate because it is present in the nearby raphé neurons (Serodio & Rudy, 1998). Any of these, or other, Kv subunits could potentially make up preBötC I_A because the voltage dependence and kinetics could be influenced by Kv channel interacting proteins (An *et al.* 2000; Rhodes *et al.* 2004) or neuromodulation (Birnbaum *et al.* 2004). However, definitive molecular level identification will require single-cell reverse transcriptase polymerase chain reaction experiments or neuroanatomical approaches.

In addition to I_A, some of the K^+ current affected by 4-AP probably includes voltage-gated K^+ channels with delayed rectifier-like properties that derive from the Kv subfamily, such as Kv2.x and Kv3.x subtypes, because 4-AP extended action potential duration.

However, the 4-AP-sensitive current is unlikely to include non-inactivating K^+ currents from the KCNQ subfamily, since we found no 4-AP-sensitive sustained currents from the relatively depolarized holding potential of −40 mV.

The prevalence of I_A in rhythmogenic preBötC neurons

To identify inspiratory neurons in the preBötC that may be important for rhythm generation Rekling *et al.* (1996*a*) measured the drive latency and proposed that the earliest neurons to activate during the respiratory cycle are important for rhythmogenesis. Furthermore, we recently showed that membrane capacitance (C_M) of 30–65 pF is correlated with early drive latency in preBötC neurons that most likely play the foremost role in rhythmogenesis (Hayes & Del Negro, 2007). Since we found that the majority, but not all, putatively rhythmogenic neurons express somatic I_A based on these criteria, our data suggest that rhythmogenic neurons do not uniformly express I_A as originally suggested (Rekling *et al.* 1996*a*). However, we cannot exclude the possibility that many of the neurons we recorded may have expressed unrecognized dendritically localized I_A as our measurements strictly depend on the quality of our somatic voltage clamp.

Since an A-current as we have described is generally lacking in expiratory neurons, but prevalent in inspiratory neurons, we hypothesize that the molecular identity of channels that give rise to I_A may be a unique functional marker for putatively rhythmogenic neurons within the preBötC.

Role of I_A *in vivo*

In the context of endogenous network activity *in vitro* E_K is approximately −71 mV, while *in vivo* it is probably closer to −98 mV – assuming 3.2 mM $[K^+]$ in the cerebrospinal fluid (Melton *et al.* 1991; cf. Richter *et al.* 1978). We therefore expect higher driving force for I_A *in vivo*, and thus the window current would have a larger hyperpolarizing influence on baseline membrane potential. This could further de-inactivate I_A between inspiratory bursts, compared to what we observe *in vitro*. In this environment, where inspiratory neurons are expected to be under intensive bombardment of excitatory and inhibitory input, I_A may play an even more substantial role in properly synchronizing respiratory rhythmic activity through its ability to rapidly activate with a large outward current and quench spurious depolarizations.

References

Aghajanian GK (1985). Modulation of a transient outward current in serotonergic neurones by α1-adrenoceptors. *Nature* **315**, 501–503.

Al-Zubaidy ZA, Erickson RL & Greer JJ (1996). Serotonergic and noradrenergic effects on respiratory neural discharge in the medullary slice preparation of neonatal rats. *Pflugers Arch* **431**, 942–949.

An WF, Bowlby MR, Betty M, Cao J, Ling HP, Mendoza G, Hinson JW, Mattsson KI, Strassle BW, Trimmer JS & Rhodes KJ (2000). Modulation of A-type potassium channels by a family of calcium sensors. *Nature* **403**, 553–556.

Andreasen M (2002). Inhibition of slow Ca^{2+}-activated K^+ current by 4-aminopyridine in rat hippocampal CA1 pyramidal neurones. *Br J Pharmacol* **135**, 1013–1025.

Armstrong CM, Gilly WF & Bernardo R (1992). Access resistance and space clamp problems associated with whole-cell patch clamping. In *Methods in Enzymology*, pp. 100–122. Academic Press, New York.

Ballanyi K, Onimaru H & Homma I (1999). Respiratory network function in the isolated brainstem-spinal cord of newborn rats. *Prog Neurobiol* **59**, 583–634.

Bianchi AL, Denavit-Saubie M & Champagnat J (1995). Central control of breathing in mammals: neuronal circuitry, membrane properties, and neurotransmitters. *Physiol Rev* **75**, 1–45.

Birnbaum SG, Varga AW, Yuan LL, Anderson AE, Sweatt JD & Schrader LA (2004). Structure and function of Kv4-family transient potassium channels. *Physiol Rev* **84**, 803–833.

Blessing WW (1997). *The Lower Brainstem and Bodily Homeostasis*. Oxford University Press, New York.

Brockhaus J & Ballanyi K (1998). Synaptic inhibition in the isolated respiratory network of neonatal rats. *Eur J Neurosci* **10**, 3823–3839.

Butera RJ Jr, Rinzel J & Smith JC (1999*a*). Models of respiratory rhythm generation in the pre-Bötzinger complex. I. Bursting pacemaker neurons. *J Neurophysiol* **82**, 382–397.

Butera RJ Jr, Rinzel J & Smith JC (1999*b*). Models of respiratory rhythm generation in the pre-Bötzinger complex. II. Populations of coupled pacemaker neurons. *J Neurophysiol* **82**, 398–415.

Byrne JH (1980). Quantitative aspects of ionic conductance mechanisms contributing to firing pattern of motor cells mediating inking behavior in *Aplysia californica*. *J Neurophysiol* **43**, 651–668.

Byrne JH, Shapiro E, Dieringer N & Koester J (1979). Biophysical mechanisms contributing to inking behavior in *Aplysia*. *J Neurophysiol* **42**, 1233–1250.

Champagnat J, Jacquin T & Richter DW (1986). Voltage-dependent currents in neurones of the nuclei of the solitary tract of rat brainstem slices. *Pflugers Arch* **406**, 372–379.

Dekin MS & Getting PA (1987). In vitro characterization of neurons in the ventral part of the nucleus tractus solitarius. II. Ionic basis for repetitive firing patterns. *J Neurophysiol* **58**, 215–229.

Dekin MS, Getting PA & Johnson SM (1987). In vitro characterization of neurons in the ventral part of the nucleus tractus solitarius. I. Identification of neuronal types and repetitive firing properties. *J Neurophysiol* **58**, 195–214.

Del Negro CA, Johnson SM, Butera RJ & Smith JC (2001). Models of respiratory rhythm generation in the pre-Bötzinger complex. III. Experimental tests of model predictions. *J Neurophysiol* **86**, 59–74.

Del Negro CA, Koshiya N, Butera RJ Jr & Smith JC (2002*a*). Persistent sodium current, membrane properties and bursting behavior of pre-Bötzinger complex inspiratory neurons in vitro. *J Neurophysiol* **88**, 2242–2250.

Del Negro CA, Morgado-Valle C & Feldman JL (2002*b*). Respiratory rhythm: an emergent network property? *Neuron* **34**, 821–830.

Del Negro CA, Morgado-Valle C, Hayes JA, Mackay DD, Pace RW, Crowder EA & Feldman JL (2005). Sodium and calcium current-mediated pacemaker neurons and respiratory rhythm generation. *J Neurosci* **25**, 446–453.

Feldman JL & Del Negro CA (2006). Looking for inspiration: new perspectives on respiratory rhythm. *Nat Rev Neurosci* **7**, 232.

Funk GD, Smith JC & Feldman JL (1993). Generation and transmission of respiratory oscillations in medullary slices: role of excitatory amino acids. *J Neurophysiol* **70**, 1497–1515.

Funk GD, Smith JC & Feldman JL (1995). Modulation of neural network activity in vitro by cyclothiazide, a drug that blocks desensitization of AMPA receptors. *J Neurosci* **15**, 4046–4056.

Gabel LA & Nisenbaum ES (1998). Biophysical characterization and functional consequences of a slowly inactivating potassium current in neostriatal neurons. *J Neurophysiol* **79**, 1989–2002.

Getting PA (1983). Mechanisms of pattern generation underlying swimming in *Tritonia*. III. Intrinsic and synaptic mechanisms for delayed excitation. *J Neurophysiol* **49**, 1036–1050.

Getting PA (1989). Emerging principles governing the operation of neural networks. *Annu Rev Neurosci* **12**, 185–204.

Gray PA, Rekling JC, Bocchiaro CM & Feldman JL (1999). Modulation of respiratory frequency by peptidergic input to rhythmogenic neurons in the preBötzinger complex. *Science* **286**, 1566–1568.

Greer JJ, Smith JC & Feldman JL (1991). Role of excitatory amino acids in the generation and transmission of respiratory drive in neonatal rat. *J Physiol* **437**, 727–749.

Gulledge AT, Kampa BM & Stuart GJ (2005). Synaptic integration in dendritic trees. *J Neurobiol* **64**, 75–90.

Haddad GG, Donnelly DF & Getting PA (1990). Biophysical properties of hypoglossal neurons in vitro: intracellular studies in adult and neonatal rats. *J Appl Physiol* **69**, 1509–1517.

Haddad GG & Getting PA (1989). Repetitive firing properties of neurons in the ventral region of nucleus tractus solitarius. In vitro studies in adult and neonatal rat. *J Neurophysiol* **62**, 1213–1224.

Hagiwara S, Kusano K & Saito N (1961). Membrane changes of *Onchidium* nerve cell in potassium-rich media. *J Physiol* **155**, 470–489.

Haller M, Mironov SL, Karschin A & Richter DW (2001*a*). Dynamic activation of K_{ATP} channels in rhythmically active neurons. *J Physiol* **537**, 69–81.

Haller M, Mironov SL & Richter DW (2001*b*). Intrinsic optical signals in respiratory brain stem regions of mice: neurotransmitters, neuromodulators, and metabolic stress. *J Neurophysiol* **86**, 412–421.

Hayes JA & Del Negro CA (2007). Neurokinin receptor-expressing pre-Bötzinger complex neurons in neonatal mice studied in vitro. *J Neurophysiol* **97**, 4215–4224.

Hess D & El Manira A (2001). Characterization of a high-voltage-activated I_A current with a role in spike timing and locomotor pattern generation. *Proc Natl Acad Sci U S A* **98**, 5276–5281.

Hoffman DA, Magee JC, Colbert CM & Johnston D (1997). K^+ channel regulation of signal propagation in dendrites of hippocampal pyramidal neurons. *Nature* **387**, 869–875.

Inyushkin AN (2005). Thyroliberin blocks the potassium A-current in neurons in the respiratory center of adult rats in vitro. *Neurosci Behav Physiol* **35**, 549–554.

Johnson SM, Smith JC & Feldman JL (1996). Modulation of respiratory rhythm in vitro: role of Gi/o protein-mediated mechanisms. *J Appl Physiol* **80**, 2120–2133.

Kosmidis EK, Pierrefiche O & Vibert JF (2004). Respiratory-like rhythmic activity can be produced by an excitatory network of non-pacemaker neuron models. *J Neurophysiol* **92**, 686–699.

Lape R & Nistri A (1999). Voltage-activated K^+ currents of hypoglossal motoneurons in a brain stem slice preparation from the neonatal rat. *J Neurophysiol* **81**, 140–148.

Marder E (2001). Moving rhythms. *Nature* **410**, 755.

Melton JE, Chae LO, Neubauer JA & Edelman NH (1991). Extracellular potassium homeostasis in the cat medulla during progressive brain hypoxia. *J Appl Physiol* **70**, 1477–1482.

Mironov SL, Langohr K, Haller M & Richter DW (1998). Hypoxia activates ATP-dependent potassium channels in inspiratory neurones of neonatal mice. *J Physiol* **509**, 755–766.

Mironov SL, Langohr K & Richter DW (1999). A1 adenosine receptors modulate respiratory activity of the neonatal mouse via the cAMP-mediated signaling pathway. *J Neurophysiol* **81**, 247–255.

Mironov SL, Langohr K & Richter DW (2000). Hyperpolarization-activated current, Ih, in inspiratory brainstem neurons and its inhibition by hypoxia. *Eur J Neurosci* **12**, 520–526.

Mironov SL & Richter DW (1998). L-type Ca^{2+} channels in inspiratory neurones of mice and their modulation by hypoxia. *J Physiol* **512**, 75–87.

Mironov SL & Richter DW (2000). Intracellular signalling pathways modulate K_{ATP} channels in inspiratory brainstem neurones and their hypoxic activation: involvement of metabotropic receptors, G-proteins and cytoskeleton. *Brain Res* **853**, 60–67.

Mironov SL & Richter DW (2001). Oscillations and hypoxic changes of mitochondrial variables in neurons of the brainstem respiratory centre of mice. *J Physiol* **533**, 227–236.

Nisenbaum ES, Xu ZC & Wilson CJ (1994). Contribution of a slowly inactivating potassium current to the transition to firing of neostriatal spiny projection neurons. *J Neurophysiol* **71**, 1174–1189.

Onimaru H, Arata A & Homma I (1997). Neuronal mechanisms of respiratory rhythm generation: an approach using in vitro preparation. *Jpn J Physiol* **47**, 385–403.

Onimaru H, Ballanyi K & Homma I (2003). Contribution of Ca^{2+}-dependent conductances to membrane potential fluctuations of medullary respiratory neurons of newborn rats *in vitro*. *J Physiol* **552**, 727–741.

Onimaru H, Kumagawa Y & Homma I (2006). Respiration-related rhythmic activity in the rostral medulla of newborn rats. *J Neurophysiol* **96**, 55–61.

Onimaru H, Shamoto A & Homma I (1998). Modulation of respiratory rhythm by 5-HT in the brainstem-spinal cord preparation from newborn rat. *Pflugers Arch* **435**, 485–494.

Paarmann I, Frermann D, Keller BU, Villmann C, Breitinger HG & Hollmann M (2005). Kinetics and subunit composition of NMDA receptors in respiratory-related neurons. *J Neurochem* **93**, 812–824.

Pace RW, Mackay DD, Feldman JL & Del Negro CA (2007*a*). Inspiratory bursts in the preBötzinger complex depend on a calcium-activated non-specific cation current linked to glutamate receptors in neonatal mice. *J Physiol* **582**, 113–125.

Pace RW, Mackay DD, Feldman JL & Del Negro CA (2007*b*). Role of persistent sodium current in mouse preBötzinger complex neurons and respiratory rhythm generation. *J Physiol* **580**, 485–496.

Pak MD, Baker K, Covarrubias M, Butler A, Ratcliffe A & Salkoff L (1991). mShal, a subfamily of A-type K^+ channel cloned from mammalian brain. *Proc Natl Acad Sci U S A* **88**, 4386–4390.

Pena F, Parkis MA, Tryba AK & Ramirez J-M (2004). Differential contribution of pacemaker properties to the generation of respiratory rhythms during normoxia and hypoxia. *Neuron* **43**, 105.

Pena F & Ramirez JM (2002). Endogenous activation of serotonin-2A receptors is required for respiratory rhythm generation in vitro. *J Neurosci* **22**, 11055–11064.

Pena F & Ramirez JM (2004). Substance P-mediated modulation of pacemaker properties in the mammalian respiratory network. *J Neurosci* **24**, 7549–7556.

Pierrefiche O, Bischoff AM & Richter DW (1996). ATP-sensitive K^+ channels are functional in expiratory neurones of normoxic cats. *J Physiol* **494**, 399–409.

Pierrefiche O, Haji A, Bischoff A & Richter DW (1999). Calcium currents in respiratory neurons of the cat in vivo. *Pflugers Arch* **438**, 817–826.

Pierrefiche O, Schwarzacher SW, Bischoff AM & Richter DW (1998). Blockade of synaptic inhibition within the pre-Bötzinger complex in the cat suppresses respiratory rhythm generation *in vivo*. *J Physiol* **509**, 245–254.

Ptak K, Zummo GG, Alheid GF, Tkatch T, Surmeier DJ & McCrimmon DR (2005). Sodium currents in medullary neurons isolated from the pre-Bötzinger complex region. *J Neurosci* **25**, 5159–5170.

Rekling JC, Champagnat J & Denavit-Saubie M (1996*a*). Electroresponsive properties and membrane potential trajectories of three types of inspiratory neurons in the newborn mouse brain stem in vitro. *J Neurophysiol* **75**, 795–810.

Rekling JC, Champagnat J & Denavit-Saubie M (1996*b*). Thyrotropin-releasing hormone (TRH) depolarizes a subset of inspiratory neurons in the newborn mouse brain stem in vitro. *J Neurophysiol* **75**, 811–819.

Rekling JC & Feldman JL (1998). PreBötzinger complex and pacemaker neurons: hypothesized site and kernel for respiratory rhythm generation. *Annu Rev Physiol* **60**, 385–405.

Rekling JC, Funk GD, Bayliss DA, Dong XW & Feldman JL (2000). Synaptic control of motoneuronal excitability. *Physiol Rev* **80**, 767–852.

Rhodes KJ, Carroll KI, Sung MA, Doliveira LC, Monaghan MM, Burke SL, Strassle BW, Buchwalder L, Menegola M, Cao J, An WF & Trimmer JS (2004). KChIPs and Kv4 α subunits as integral components of A-type potassium channels in mammalian brain. *J Neurosci* **24**, 7903–7915.

Richter DW, Camerer H & Sonnhof U (1978). Changes in extracellular potassium during the spontaneous activity of medullary respiratory neurones. *Pflugers Arch* **376**, 139–149.

Richter DW & Spyer KM (2001). Studying rhythmogenesis of breathing: comparison of in vivo and in vitro models. *Trends Neurosci* **24**, 464–472.

Rogawski MA (1985). The A-current: how ubiquitous a feature of excitable cells is it? *Trends Neurosci* **8**, 214–219.

Ruangkittisakul A, Schwarzacher SW, Secchia L, Poon BY, Ma Y, Funk GD & Ballanyi K (2006). High sensitivity to neuromodulator-activated signaling pathways at physiological $[K^+]$ of confocally imaged respiratory center neurons in on-line-calibrated newborn rat brainstem slices. *J Neurosci* **26**, 11870–11880.

Rusch A & Eatock RA (1996). A delayed rectifier conductance in type I hair cells of the mouse utricle. *J Neurophysiol* **76**, 995–1004.

Rybak IA, Paton JF & Schwaber JS (1997). Modeling neural mechanisms for genesis of respiratory rhythm and pattern. I. Models of respiratory neurons. *J Neurophysiol* **77**, 1994–2006.

Rybak IA, Shevtsova NA, Ptak K & McCrimmon DR (2004). Intrinsic bursting activity in the pre-Bötzinger complex: role of persistent sodium and potassium currents. *Biol Cybern* **90**, 59–74.

Rybak IA, Shevtsova NA, St-John WM, Paton JF & Pierrefiche O (2003). Endogenous rhythm generation in the pre-Bötzinger complex and ionic currents: modelling and in vitro studies. *Eur J Neurosci* **18**, 239–257.

Serodio P, Kentros C & Rudy B (1994). Identification of molecular components of A-type channels activating at subthreshold potentials. *J Neurophysiol* **72**, 1516–1529.

Serodio P & Rudy B (1998). Differential expression of Kv4 K^+ channel subunits mediating subthreshold transient K^+ (A-type) currents in rat brain. *J Neurophysiol* **79**, 1081–1091.

Serodio P, Vega-Saenz de Miera E & Rudy B (1996). Cloning of a novel component of A-type K^+ channels operating at subthreshold potentials with unique expression in heart and brain. *J Neurophysiol* **75**, 2174–2179.

Shao XM & Feldman JL (2000). Acetylcholine modulates respiratory pattern: effects mediated by M3-like receptors in preBötzinger complex inspiratory neurons. *J Neurophysiol* **83**, 1243–1252.

Shao XM, Ge Q & Feldman JL (2003). Modulation of AMPA receptors by cAMP-dependent protein kinase in preBötzinger complex inspiratory neurons regulates respiratory rhythm in the rat. *J Physiol* **547**, 543–553.

Smith JC, Ellenberger HH, Ballanyi K, Richter DW & Feldman JL (1991). Pre-Bötzinger complex: a brainstem region that may generate respiratory rhythm in mammals. *Science* **254**, 726–729.

Stein PSG (1997). *Neurons, Networks, and Motor Behavior*. MIT Press, Cambridge.

Storm JF (1988). Temporal integration by a slowly inactivating K^+ current in hippocampal neurons. *Nature* **336**, 379–381.

Thoby-Brisson M, Telgkamp P & Ramirez JM (2000). The role of the hyperpolarization-activated current in modulating rhythmic activity in the isolated respiratory network of mice. *J Neurosci* **20**, 2994–3005.

Tierney AJ & Harris-Warrick RM (1992). Physiological role of the transient potassium current in the pyloric circuit of the lobster stomatogastric ganglion. *J Neurophysiol* **67**, 599–609.

Trimmer JS & Rhodes KJ (2004). Localization of voltage-gated ion channels in mammalian brain. *Annu Rev Physiol* **66**, 477–519.

Viana F, Bayliss DA & Berger AJ (1993). Multiple potassium conductances and their role in action potential repolarization and repetitive firing behavior of neonatal rat hypoglossal motoneurons. *J Neurophysiol* **69**, 2150–2163.

Acknowledgements

This work was supported by the National Science Foundation, Integrative and Organismal Biology Award no. 0616099 (Arlington, VA, USA), The Suzann Wilson Matthews Faculty Research Award (The College of William and Mary), and The Jeffress Memorial Trust (Richmond, Virginia, USA). J.A.H. and B.R.B. were funded (in part) by the postdoctoral and undergraduate biological sciences education program grant awarded to The College of William and Mary by the Howard Hughes Medical Institute.